Loading of Antibiotic into Biocoated Hydroxyapatite Nanoparticles: Smart antitumor platforms with Regulated Release

Manuel Rivas[1], Luís J. del Valle[1,2], Anna M. Rodríguez-Rivero,[3] Pau Turon[3*], Jordi Puiggalí[1,2*] and Carlos Alemán[1,2*]

[1] *Departament d'Enginyeria Química, EEBE, Universitat Politècnica de Catalunya, C/ Eduard Maristany, 10-14, 08930, Sant Adriá del Besòs, Spain.*

[2] *Center for Research in Nano-Engineering, Universitat Politècnica de Catalunya, Campus Sud, Edifici C', C/Pasqual i Vila s/n, Barcelona E-08028, Spain*

[3] *B. Braun Surgical, S.A. Carretera de Terrasa 121, 08191 Rubí (Barcelona), Spain*

*Correspondence to: pau.turon@bbraun.com, jordi.puiggali@upc.edu and carlos.aleman@upc.edu

ABSTRACT

In this research we propose a nanoplatform for anticancer therapy that is based on the combination of three components: 1) an antibiotic to target selectively the mitochondria of cancer cells, inhibiting their functions; 2) mineral nanoparticles (NPs) able to encapsulate the antibiotic and to enter into the cells across the cell membrane; and 3) a biocoating to protect the antibiotic during and/or after its regulated release, increasing its therapeutic efficacy. Chloramphenicol (CAM), a prototypical wide-spectrum antibiotic, has been used to induce mitochondrial-dysfunctions in cancer cells. Different *in situ* synthetic strategies have been tested to load such antibiotic into both crystalline hydroxyapatite (cHAp) and amorphous calcium phosphate (ACP) NPs. cHAp NPs showed higher loading capacity, in terms of encapsulation and superficial adsorption of CAM, and slower antibiotic release than ACP NPs. On the other hand, the protecting role played by biocoatings based on pyrophosphate and, especially, triphosphate was greater than biophosphonates, the anticancer therapeutic efficacy of CAM being maximized by the formers. In vitro studies using healthy and cancer cell lines have demonstrated that *in situ* CAM-loaded cHAp NPs coated with triphosphate selectively kill a great population of cancer cells, evidencing the potential of this nanoplatform in cancer treatment.

Keywords: Antibiotic; Biocoating; Calcium phosphate; Cancer cells; Chloramphenicol; Polyphosphate

INTRODUCTION

Bone is a calcified tissue composed of 50 to 70% mineral, 20 to 40% organic matrix, 5 to 10% water, and <3% lipids. The mineral content of bone is mostly hydroxyapatite (HAp) [$Ca_{10}(PO_4)_6(OH)_2$], with small amounts of carbonate, magnesium, and acid phosphate. Compared to geologic HAp crystals, bone HAp crystals are very small, measuring only approximately 200 nm in their longest dimension. The solubility of these small crystals is higher than that of geologic HAp crystals, allowing them to support metabolism. Currently, synthetic HAp is one of the most widely used biomaterials for reconstruction of the skeleton due to the lack of local or systemic toxicity in combination with its osteoconductive properties.[1-6]

On the other hand, antibiotics that target bacterial ribosome have a common mechanism of action: they are protein synthesis inhibitors.[7] The main target for such group of antibiotics is the peptidyl transferase center,[8] which forms peptide bonds between adjacent amino acids using tRNA during the protein biosynthesis.[9] Accordingly, the therapeutic success of ribosomal antibiotics killing bacteria is based on the discrimination between prokaryotic and eukaryotic ribosome structures, which exhibit differences in size, sequence, structure, and the ratio of protein to RNA.[10,11] Chloramphenicol (CAM) is a prototypical wide-spectrum antibiotic that obstructs protein synthesis and blocks essential ribosomal functions.[12-14] CAM consists of a *p*-nitrophenyl ring attached to a dichloroacetyl tail via a 2-amino-1,3-propanediol moiety (Scheme 1). Thus, CAM incorporates itself to the C-terminus of a growing peptide chain, causing the premature release of the incomplete peptide.

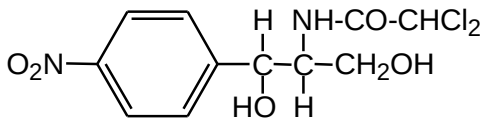

Scheme 1

On the other hand, a growing body of experimental evidences has shown that some antibiotics may inhibit mitochondrial functions of eukaryotic cells, causing changes at both molecular and physiological levels that affect the life and death of cells.[15,16] This has been attributed to the fact that mitochondrial ribosomes resemble many features of bacterial ribosomes. The metabolism of cancer cells, especially of cancer stem cells, is fundamentally regulated by an abundance of mitochondria compared to normal cells, including normal stem cells.[17] Thus, the low energy efficiency of the mostly anaerobic metabolism of cancer cells is compensated with more mitochondria than normal cells, which exhibit an aerobic metabolism. Accordingly, clinical oncologists have recently proposed the use of antibiotics as a part of anticancer therapy and target cancer metabolisms.[17-20] Within this context, in a recent study Lisante *et al.*[17] proved that CAM inhibits the formation of tumor stem cells, which are the responsible of metastasis by giving growth to new tumors.[21] The anticancer activity of CAM and other antibiotics reached great repercussion for its implications in clinical oncology.[18]

Synthetic HAp has an enormous capacity not only to encapsulate biomolecules (*e.g.* nucleic acids and proteins[22,23]) but also to adsorb a variety bio-organic and inorganic chemical species (*e.g.* DNA,[24] amino acids,[25,26] phosphate- and biophosphonate-derivatives[27]). HAp-based platforms have been used for bone regeneration through adsorbing inorganic polyphosphates from the metabolism onto the mineral,[28-31] for the fight against different bone diseases (*e.g.* osteoporosis, Paget disease of bone and malignancies metastatic to bone) through the delivery of biophosphonates as pharmacological agents,[32,33] and for gene delivery by transfecting cells, as HAp is able to adsorb, transport and deliver nucleic acids inside the cell nucleus.[24,34,35]

The current study focuses on antitumoral nanoplatforms that combine the ability of CAM to inhibit the mitochondrial functions and the capacity of HAp to encapsulate

biomolecules and enter into cells. For this purpose, CAM-loaded mineral nanoparticles (NPs) covered with an inorganic biocoating have been prepared and characterized. After this, we have demonstrated that such biocoated CAM-containing systems satisfy the most important criteria required by therapeutic nanoplatforms (*e.g.* the loaded antibiotic preserves the bioactive conformation and its release is regulated by the physical properties of both the NPs and the biocoating). Finally, different inhibitory effects of the proposed antitumoral nanoplatforms have been examined on both normal cells (HUVEC endothelial line and COS-1 fibroblast line) and cancer cells (MCF-7 breast cancer line and MIA PaCa-2 pancreas cancer line). The selectivity of biocoated HAp NPs loaded with CAM on killing cancer cells proves their potential application in cancer treatment.

RESULTS AND DISCUSSION

Chloramphenicol-loaded hydroxyapatite: Preparation and characterization

Because of their different characteristics and properties, both crystalline HAp (cHAp) and amorphous calcium phosphate (ACP) NPs have been considered for this study. The experimental conditions used to prepare unloaded cHAp and ACP NPs[24,27] were adapted for the *in situ* loading of CAM. In both cases a 0.5 M $(NH_4)_2HPO_4$ aqueous solution was added drop-wise and under agitation to a 0.5 M $Ca(NO_3)_2$ ethanol solution, reagents being adjusted to get a Ca/P ratio of 1.67. The resultant suspension was aged for 24 h at 37 ºC to produce ACP, whereas cHAp was obtained by applying hydrothermal conditions during 24 h. Details of the experimental conditions and procedures are provided in the Supporting Information.

CAM-loaded NPs were prepared using four different *in situ* loading strategies: 2 minerals (cHAp or ACP) × 2 loading paths of the antibiotic into the corresponding

$(NH_4)_2HPO_4$ or $Ca(NO_3)_2$ feeding solution (Pho- or Ca-path, respectively) = 4 strategies. The nomenclature used for the resulting NPs is indicated in Figure 1a.

The loading efficiency (LEff), which is expected to be sensitive to the path because of the different strength of CAM$\cdots PO_4^{3-}$ and CAM$\cdots Ca^{2+}$ interactions, was evaluated by UV-vis spectroscopy. The *in situ* loading strategies used in this work cause both the entrapment of CAM inside the mineral matrix (*i.e.* encapsulation or mineralization) and the adsorption of CAM on the surface mineral NPs. In order to distinguish between such two situations, the LEff was determined considering: (*i*) the CAM extracted from the mineral surface by washing with a phosphate buffered saline (PBS) solution supplemented with 70% v/v ethanol (PBS-EtOH) during several hours; and (*ii*) the CAM encapsulated into mineral NPs that, after washing as in (*i*), were dissolved in a 100 mM HCl : 50 mM NaCl mixture. The UV-vis spectra of samples coming from (*i*) and (*ii*) showed the absorption band of the *p*-nitrophenyl chromophore (Scheme 1) at around 278 nm.[36] The intensity of the peaks increased gradually with the CAM concentration enabling calibration in a linear model (Figure S1).

The sensitivity of the CAM distribution to the path is reflected in Figure 1b, which represents the weight ratio of adsorbed and encapsulated antibiotic with respect to the dry weight of mineral. The amount of CAM loaded through the Ca-path was greater than through the Pho-path for both cHAp and ACP. This difference mainly arises from the encapsulated antibiotic since the concentration of adsorbed CAM is similar for both ACP and cHAp NPs. This feature is consistent with the similar surface areas found for both kind of NPs.[24] Accordingly, hereafter discussion of the results have been mainly focused on CAM(Ca)-loaded cHAp and ACP NPs.

Control NPs, denoted CAM(c)/cHAp and CAM(c)/ACP, were prepared using an *ex situ* loading approach: deposition of 500 μL of 150 mM CAM solution onto 50 mg of

already synthetized cHAp and ACP NPs, respectively. The distribution of the accumulated antibiotic was completely different from those found for *in situ* loaded NPs (Figure S2): the amount of CAM that penetrated into the mineral matrix for encapsulation was significantly smaller than the antibiotic adsorbed on the surface.

Figure 2a compares the FTIR spectra recorded for CAM alone, unloaded cHAp NPs, CAM(Ca)/cHAp NPs as prepared (*i.e.* with both adsorbed and encapsulated CAM), and CAM(Ca)/cHAp NPs after eliminate the antibiotic adsorbed onto the surface washing with PBS-EtOH (*i.e.* with encapsulated CAM only). The characteristic bands of cHAp (at around 1021 cm^{-1})[24] and of CAM (3350-1300 cm^{-1} interval)[37] appear in the spectra recorded for CAM(Ca)/cHAp NPs as prepared and washed with PBS-EtOH. Thus, presence of CAM is proved by the absorption peaks at 3332 (O–H stret), 3248 (N–H stret), 3080 (C–H stret), 1683 / 1563 (amide I / amide II of the 2,2-dichlor-acetamide moiety), and 1515 / 1342 cm^{-1} (nitro / nitro-phenyl group). The absorption peaks of CAM in loaded ACP samples were detected at very similar positions (Figure S3).

Results from the characterization of unloaded and CAM(Ca)-loaded mineral NPs by XRD are summarized in Figure 2b and Table 1. The reflections identified for CAM alone (Figure S4) are fully consistent with those reported in the literature for the crystal structure of most stable antibiotic form (*alicyclic* CAM).[38,39] The most intense reflections, which correspond to the (401) and (114) planes with *d*-spacing 0.428 nm, together with the (002) (*d*= 1.108 nm), (201) (*d*= 0.815 nm), (202) (*d*= 0.687 nm) and (203) (*d*= 0.564 nm), allow identification of the antibiotic in the loaded NPs, since the rest of the peaks overlap with characteristic reflections of cHAp and ACP.

Both the crystallinity and the crystallite size are lower for CAM-loaded ACP and, especially, cHAp samples than for the unloaded ones (Table 1). This observation reflects that the antibiotic affects the formation of crystallization nuclei, reducing both

their number and size. This phenomenon has been attributed to the competition between CAM···mineral interactions and CAM intramolecular hydrogen bonds, the latter being characteristic of the alicyclic form of the antibiotic (see next sub-section). The difficulties in the formation of CAM···mineral interactions and the stability of the alicyclic CAM preclude the role of the antibiotic as nucleating agent. Furthermore, the incorporation of the antibiotic to the mineral matrix causes steric hindrance, inhibiting the growth of already formed crystallization nuclei.

SEM and TEM micrographs of CAM alone and CAM(Ca)-loaded mineral NPs, after elimination of the antibiotic at the surface with PBS-EtOH, are displayed in Figure 3. CAM is a crystalline antibiotic that organizes in nanoplates (Figure 3a). The nanospherical and nanorod-like morphologies of CAM(Ca)/ACP (Figure 3b) and CAM(Ca)/cHAp (Figure 3c), respectively, are similar to those of unloaded minerals,[22] evidencing that the encapsulation of the antibiotic does not modify the morphology of the NPs. Accordingly, the loading strategy promotes the homogeneous integration of the antibiotic into the mineral matrix during the biomineralization process.

In previous work we described the ability of both ACP and cHAp to adsorb biophosphates (*e.g.* pyrophosphates and triphosphates, abbreviated $P_2O_7^{4-}$ and polyP, respectively) and biophosphonates (*e.g.* amino-tris(methylenephosphonic acid), abbreviated ATMP),[24] which are important for bone regeneration. Such bioadsorption capacity has been used in this study to protect the loaded antibiotic during the delivery process.

Figure 4 displays SEM micrographs of CAM(Ca)/ACP and CAM(Ca)/cHAp samples after incubation with $P_2O_7^{4-}$, polyP or ATMP solutions, as described in the Supporting Information. Comparison with micrographs displayed in Figure 3 reflects the formation of superficial protecting layers. The significant morphological changes have been

attributed to the fact that, after the first stages of the bioadsorption process, a surface-induced crystal growing process occurred for the three biocoatings. On the other hand, quantification of the adsorbed and encapsulated amount of CAM indicates that the biocoating does not interfere with the loaded antibiotic and, therefore, does not induce its premature release during the bioadsorption process (Figure S5). FTIR and X-ray diffraction studies (Figures S6-S10, and Table S1) confirmed the presence of the biocoating and its negligible influence in the internal structure of CAM-loaded mineral samples.

Effect of the loading in the bioactivity of CAM

The alicyclic form of CAM has been associated to its antimicrobial action.[40] In this bioactive conformation the hydroxyl groups of the antibiotic are engaged in closing an alicyclic ring by hydrogen bonding (Scheme 2). Accordingly, the activity of CAM could be altered by structural changes that affect the functional character of such hydroxyl groups. In this sub-section, we examine the effect of CAM···mineral interactions in the bioactive response of the antibiotic.

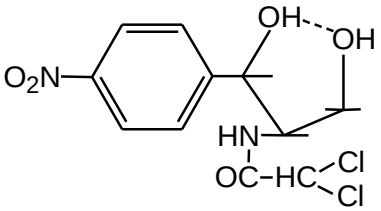

Scheme 2

As mentioned above, the peaks identified in the diffractograms recorded for CAM(Ca)/cHAp and CAM(Ca)/ACP NPs before (Figure 2a) and after applying biocoatings (Figures S9 and S10) correspond to those identified for the crystal structure of CAM (Figure S4). Accordingly, the crystalline structure of the antibiotic remains

unaltered during both the loading and coating processes. In addition, the position of the O–H absorption band in the FTIR spectra is the same for the antibiotic alone and loaded (Figures 2a, S3 and S6-S8). Thus, the alicyclic ring is apparently unaltered by the formation of CAM···mineral, CAM···biocoating and mineral···biocoating interactions, which suggests that the antibiotic is not forming specific hydrogen bonding interactions with the mineral and/or the biocoating.

In order to confirm that the bioactive conformation of CAM was not altered by the loading and bioadsorption processes, the activity of the loaded antibiotic loaded was tested against representative Gram-negative bacteria (*E. coli*) and compared with that of free antibiotic. Figure 5a plots the relative growth rate of the partially inhibited cultures against the logarithm of the antibiotic concentration for free CAM, CAM(Ca)/cHAp and CAM(Ca)/ACP. Symmetrical sigmoid curves similar to the dose-response curves of many biological systems were obtained in all cases. The central portion of the curve approaches linearity, allowing a graphic extrapolation of the 50% growth inhibition levels. The half maximal inhibitory concentration (IC_{50}) of antibiotic determined for free CAM, CAM(Ca)/cHAp and CAM(Ca)/ACP is 0.96, 0.94 and 0.94 μg/mL, respectively, reflecting that the bioactivity of CAM is preserved in loaded mineral NPs. Figure 5b and 5c compares the bacterial growth inhibition of uncoated and biocoated CAM(Ca)/cHAp and CAM(Ca)/ACP NPs, respectively. It is worth noting that the bioadsorption of polyP, $P_2O_7^{4-}$ and ATMP does not alter the inhibitory characteristics of the antibiotic, evidencing that CAM preserves the bioactive conformation.

CAM-Release in PBS and cell culture media

Quantitative release assays in the simplest physiological medium, PBS, were performed with CAM(Ca)/cHAp and CAM(Ca)/ACP NPs, CAM(c)/cHAp and

CAM(c)/ACP NPs being used as controls. Results displayed in Figure 6a indicate that, although the amount of loaded antibiotic was entirely released after ~72 h in all cases, the release rate was slower for CAM(Ca)/cHAp than for CAM(Ca)/ACP. More specifically, the time necessary to release 50% of loaded CAM (t_{50}) was ~23 and ~7 h respectively. On the other hand, the release rate was significantly faster for control NPs than for minerals loaded using the *in situ* approach (*i.e.* $t_{50}\approx$ 12 and 4 h for CAM(c)/cHAp and CAM(c)/ACP, respectively), evidencing that the encapsulation achieved by the latter procedure exerts a regulating effect. The sustained antibiotic release observed for the *in situ* loaded NPs has been attributed to the slow diffusion of the encapsulated CAM through the mineral matrix.

The behavior of CAM(Ca)-loaded mineral NPs coated with polyP, $P_2O_7^{4-}$ and ATMP (Figures 6b-d) was similar to that described for the uncoated systems. The antibiotic release rate was faster for ACP than for cHAp, independently of the coating. Furthermore, the release rate was faster for control NPs than for those loaded using the *in situ* approach. Quantitative comparison between uncoated and coated CAM(Ca)/cHAp reflects that the release rate is the same for uncoated and polyP-coated NPs (*e.g.* $t_{50}\approx$ 23 h in both cases), whereas $P_2O_7^{4-}$ and, specially, ATMP biocoatings tend to accelerate the delivery process (*e.g.* $t_{50}\approx$ 20 and 17 h, respectively).

Antibiotic release assays from uncoated and coated CAM(Ca)/cHAp and CAM(Ca)/ACP NPs were also carried out in cell culture media using three different cell lines: human umbilical vein endothelial cells (HUVEC), green monkey kidney fibroblast cells (COS-1), and human breast cancer cells (MCF-7). The release profiles, which are displayed in Figures 7 and S11, were very similar to those obtained in PBS. Thus, the retardation effect increased with the crystallinity of the sample, the release from cHAp NPs being slower than from ACP NPs. These characteristic trends were also

identified for biocoated NPs, the influence of the chemical specie adsorbed at the surface of the mineral NPs being practically negligible. However, the most important result is that the antibiotic release profiles obtained for uncoated and biocoated CAM(Ca)/cHAp and CAM(Ca)/ACP NPs are totally independent of cell line.

The sustained release of CAM displayed *in vitro* by both cHAp and ACP, which is not affected by the biological environment, suggests that such mineral NPs could act as antitumoral nanoplatforms for *in vivo* treatments. More specifically, our results clearly indicate that cHAp and ACP NPs act as efficient vehicles for the CAM transport and delivery.

Can CAM-loaded mineral NPs be used to fight cancer cells?

In previous sub-sections, we proved that cHAp and ACP NPs prepared using the *in situ* Ca-path are efficient platforms for the loading of bioactive CAM and its delayed release with respect to platforms prepared using the usual *ex situ* incubation approach. In this section, we examine the response of cells to CAM(Ca)/cHAp and CAM(Ca)/ACP NPs. Initially, an exploratory study was conducted using the electroporation technique to facilitate the permeation of CAM-loaded mineral NPs across cell membranes, since the anticancer therapy using antibiotics is based on the targeting of mitochondria.[15-18] Electroporation is the increment of the cell membrane permeability by exposing the cells to short electric current pulses from an external source. Such increase in permeability, which is related with the formation of nanoscale defects or pores in the cell membrane, allows the direct physical transfer of numerous kinds of chemical species into cells. In our case, we use this effect to ensure the entry of the NPs into the cells.

Unloaded and CAM-loaded mineral NPs, without and with biocoating, were introduced in culture media with non-cancerous (HUVEC and COS-1) and cancerous (MCF-7) cells, which were electroporated to facilitate the internalization process. A sub-lethal dose of CAM was used in these assays in order to avoid generalized cytotoxicity (*i.e.* a dose that will kill less than 5% of the test cells) and allow the population of unaffected cells to recover over time. Then, they were seeded in the culture plate and evaluated at different times. In order to investigate the effects of the antibiotic in living cells, the viability was determined through the MTT [3-(4,5-dimethylthiazol-2-yl)-2,5-diphenyltetrazolium bromide] assay. The cytotoxic response of HUVEC, COS-1 and MCF-7 cell lines exposed to the increasing concentrations of CAM is displayed in Figure 8.

As it was expected due to the use of sub-lethal doses, electroporated cells remained practically unaffected after the internalization of unloaded cHAp and ACP NPs (Figures S12 and S13, respectively), independently of both the cell type and the biocoating. Plots representing the variation of survival cells with time indicate an immediate reduction of the viability. This effect, which is frequently observed after the incorporation of agents extraneous to the culture medium, has been associated to the high concentration of mineral NPs and, therefore, to the high content of Ca^{2+} inside the electroporated cells. After this initial effect, cells recover in number over time until reach ~100% of the initial viability after 120 h.

Addition of uncoated and biocoated CAM(Ca)/HAp NPs into non-cancerous cell models, HUVEC and COS-1 (Figures 9a and 9b, respectively), caused an almost identical response. Thus, the fraction of surviving non-cancerous cells after 120 h was 100%, evidencing that CAM is not inhibiting mitochondrial functions and, therefore, preserving the cell viability. In contrast, CAM(Ca)/HAp NPs damaged MCF-7

cancerous cells (Figure 9c), causing a high percentage of cells to die (39%±5%). The different response of normal and cancer cells against CAM(Ca)-loaded mineral NPs is due to a combination of two factors: (*i*) mitochondria are more abundant in cancerous cells than in non-cancerous cells;[17] and (*ii*) the similarity between bacterial and mitochondrial ribosomes.[15]

As CAM(Ca)-loaded cHAp NPs are very toxic for cancer cells as compared to innocuous unloaded cHAp, protection of the antibiotic using biocoatings is expected to enhance such destructive effects. Effectively, the percentage of surviving cells drops drastically for CAM(Ca)/cHAp NPs coated with polyP, $P_2O_7^{4-}$ and ATMP (Figure 9c). More specifically, after 120 h the percentage of dead cells increased from 39%±5% for uncoated NPs to 59%±3% (polyP), 51%±5% ($P_2O_7^{4-}$) and 51%±4% (ATMP) for coated NPs. These results indicate that the protecting role exerted by the biocoating, especially by polyP, enhances the efficiency of the antibiotic as anticancer agent. According to previous discussion (Figure 8), this phenomenon cannot be attributed to a delay in the release of the antibiotic (*i.e.* release curves for uncoated and biocoated CAM(Ca)-loaded NPs were very similar). Instead, two different hypotheses can be considered two explain the protection offered by the biocoating: (1) CAM···biocoating complexes allow to protect the antibiotic molecules against enzymatic degradation, avoiding the premature reduction in the amount of effective CAM as anticancer agent. More specifically, acetyltransferases covalently modify CAM resulting in structural alterations (*i.e.* O-acetylation through deprotonation of the hydroxyl group) that impair target binding;[41] and (2) the dissolved biocoating molecules capture the antibiotic ones, transporting them to the mitochondria to enhance the antitumor activity (*i.e.* they act as targeted carriers).

In order to ascertain if the protecting role attributed to the biocoating affects to the CAM adsorbed onto mineral NPs only or extends to the antibiotic encapsulated into the cHAp matrix, additional assays were performed by introducing uncoated and biocoated CAM(c)/HAp NPs into electroporated HUVEC, COS-1 and MCF-7 cells. The population of surviving HUVEC and COS-1 cells after 120 h was 100% (Figure S14) while the amount of MCF-7 cells decreased (Figure 9d). However, such reduction was not only smaller than that observed for CAM(Ca)/cHAp but also independent of the presence of biocoating. Thus, the percentage of dead MCF-7 cells after 120 h is 34%±4% for uncoated CAM(c)/cHAp, remaining at 35%±5% , 32%±3% and 32%±5% for NPs coated with polyP, $P_2O_7^{4-}$ and ATMP, respectively. Comparison of results displayed in Figures 9c and 9d indicates that CAM molecules biomineralized inside the cHAp matrix through the *in situ* polymerization approach play a crucial role in the success of biocoated CAM(Ca)/cHAp NPs as antitumoral platforms. Thus, the biocoating layer probably prevents from degradation before the internalization of the NPs, increasing the therapeutic efficacy of CAM.

Qualitative analysis of the results obtained for CAM(Ca)/ACP (Figure S15a-c) and CAM(c)/ACP (Figures S15d and S16) reflected a similar behavior. After 120 h, 100% of non-cancerous cells survived, while the percentage of dead MCF-7 cells grew from 22%±3% for uncoated CAM(Ca)/ACP to 44%±4% (polyP), 33%±4% ($P_2O_7^{4-}$) or 33%±2% (ATMP) for coated NPs. From a quantitative point of view, the antitumor efficacy of the loaded antibiotic is around 15-20% higher for cHAp than for ACP, independently of the biocoating. This feature has been attributed to the fact that the release from CAM(Ca)/cHAp is slower than from CAM(Ca)/ACP.

Proving the antitumor efficacy of CAM-loaded mineral nanoparticles via endocytic pathway

The last aspect to be addressed in this work refers to the cellular uptake of biocoated CAM(Ca)/cHAp NPs from the surrounding fluid without artificially created transient pores at the cell membrane (*i.e.* without apply electroporation). Endocytosis is the form of active transport used by almost all living eukaryotic cells to internalize extracellular materials that cannot pass through the membrane by simple diffusion. It is known that HAp enters into cells through the endocytic pathway.[42-44] As the endocytosis activity of cancer cells is greater than that of normal cells,[45-47] in this section we focus on the effect of both the biocoating and the loaded antibiotic in the efficiency of the endocytic process, which is expected to be closely related with the antitumor efficacy of the proposed therapeutic platforms.

The effect of the incorporation of unloaded cHAp particles into the cell culture was practically nil (Figure S17), the amount of surviving HUVEC, COS-1 and MCF-7 cells after 120 h being around 100%, independently of the biocoating. In contrast, the incorporation of biocoated cHAp NPs loaded with a sub-lethal dose of CAM (Figure 10) inhibits selectively the viability of MCF-7 cancerous cells, while the response of HUVEC and COS-1 noncancerous cells is the same that for unloaded cHAp (*i.e.* ~100% of surviving cells after 120 h). The inhibitory effects of CAM(Ca)/cHAp are severely affected by both presence and chemical nature of the biocoating, such dependence being considerably more pronounced than that observed in the previous sub-section for permeable electroporated cells. Thus, although for uncoated CAM(Ca)/cHAp the percentage of dead MCF-7 cells was 26±5% after 48 h, 98% of the cell viability was recovered after 120 h (Figure 10c). Comparison of the surviving cells profiles obtained by contacting uncoated CAM(Ca)/cHAp with electroporated and non-electroporated

MCF-7 cells (Figures 9c and 10c, respectively) indicates that, in the latter case, the antibiotic release occurs mostly prior to the internalization of the NP. The apparition of temporary pores in cell membranes during the application of the electric field favors the rapid uptake of the CAM(Ca)/cHAp particles, ensuring the effectivity of the antibiotic released inside the cells once the cell membrane reseals after electroporation. In contrast, the anticancer efficacy of the antibiotic loaded in uncoated NPs is drastically limited by the rate of the endocytic process in absence of electroporation.

In opposition, biocoated CAM(Ca)/cHAp NPs improves the antitumor effectivity in absence of electroporation (Figure 10c). More specifically, the percentage of dead cancerous cells after 120 h is 58±5%, 50±5% and 46±5% for NPs coated with polyP, $P_2O_7^{4-}$ and ATMP, respectively. Accordingly, the barrier effect exerted by the biocoating with respect to the antibiotic release eliminates the rate of the endocytic as limiting step of its antitumor efficacy. The effectivity of such blocking effect varies as follows: polyP > $P_2O_7^{4-}$ > ATMP, indicating that CAM(Ca)/cHAp coated with polyP is the most effective antitumor platform.

In order to corroborate the performance of biocoated CAM(Ca)/cHAp NPs as smart antitumor platforms, additional experiments were conducted using MIA PaCa-2 pancreas cancer cells. Results, which are displayed in Figure 10d, show that the percentage of dead cancerous cells after 120 h is 54±6%, 46±5% and 41±5% for CAM(Ca)/cHAp NPs coated with polyP, $P_2O_7^{4-}$ and ATMP, respectively. These values are fully consistent with those obtained using MCF-7 cells (Figure 10c), confirming not only the barrier effect exerted by the biocoating but also the antitumor efficacy of antibiotic when it is appropriately released.

CONCLUSIONS

In the present study, we prove the very high antitumor activity of the following system: CAM loaded into cHAp NPs and, subsequently, coated with polyP. The efficiency and selectivity of CAM(Ca)/cHAp NPs coated with polyP have been demonstrated by the reduction of cancerous cells and the surviving of normal cells. The preparation strategy is essential to maximize the anticancer properties of that nanoplatform. Firstly, the *in situ* synthesis allows not only adsorbing antibiotic onto the NPs but also encapsulating CAM into the mineral matrix. Secondly, the amount of encapsulated antibiotic is higher for the Ca-path than for the Pho-path. Thirdly, hydrothermal conditions to produce cHAp are preferred with respect to aging conditions to obtain ACP. This is because the antibiotic release from cHAp is slower than from ACP, allowing a greater control of the antitumor activity. Although the biocoating is not affecting the antibiotic release process, its presence causes a drastic reduction in the amount of surviving cancer cells. Several hypotheses have been proposed to explain the role of polyP (*e.g.* as antibiotic carrier to target mitochondria or as antibiotic protector against degradation), even though more work is necessary is to provide complete understanding of the experimental observations related with the biocoating. In summary, CAM(Ca)/cHAp NPs coated with polyP in are promising bioplatforms for cancer therapy.

ACKNOWLEDGEMENTS

This work was supported by B. Braun Surgical S.A. through a joint research agreement with UPC, the MINECO/FEDER (MAT2015-69367-R and MAT2015-69547-R) and the Agència de Gestió d'Ajuts Universitaris i de Recerca (2017SGR359).

Support for the research of C.A. was received through the prize "ICREA Academia" for excellence in research funded by the Generalitat de Catalunya.

REFERENCES

1. Pina, S.; Oliveira, J. M.; Reis, L. R. Natural-Based Nanocomposites for Bone Tissue Engineering and Regenerative Medicine: A Review. *Adv. Mater.* **2015**, *27*, 1143-1169. DOI: 10.1002/adma.201403354

2. Cunniffe, G. M.; Curtin, C. M.; Thompson, E. M.; Dickson, G. R.; O'Brien, F. J. Content-Dependent Osteogenic Response of Nanohydroxyapatite: An in Vitro and in Vivo Assessment within Collagen-Based Scaffolds. *ACS Appl. Mater. Interfaces* **2016**, *8*, 23477-23488. DOI: 10.1021/acsami.6b06596

3. Lopa, S.; Henning, M. Bioinspired Scaffolds for Osteochondral Regeneration. *Tissue Eng. Part A* **2014**, *20*, 2052-2076. DOI: 10.1089/ten.tea.2013.0356

4. Bekatesan, J.; Kim, S.-K. Nano-Hydroxyapatite Composite Biomaterials for Bone Tissue Engineering – A Review. *J. Biomed. Nanotech.* **2014**, *10*, 3124-3140. DOI: doi.org/10.1166/jbn.2014.1893

5. Zakaria, S. M.; Sharif, S. H.; Othman, M. R.; Yang, F.; Jansen, J. A. Nanophase Hydroxyapatite as a Biomaterial in Advanced Hard Tissue Engineering: A Review. *Tissue Eng. Part B Rev.* **2013**, *19*, 431-441. DOI: 10.1089/ten.TEB.2012.0624

6. Scaglione, S.; Giannoni, P.; Bianchini, P.; Sandri, M.; Marotta, R.; Firpo, G.; Valbusa, U.; Tampieri, A.; Diaspro, A.; Bianco, P.; Quarto, R. Order versus Disorder: In Vivo Bone Formation within Osteoconductive Scaffolds. *Sci. Rep.* **2012**, *2*, 274. DOI: 10.1038/srep00274

7. Wilson, D. N. Ribosome-Targeting Antibiotics and Mechanisms of Bacterial Resistance. *Nature Rev. Microbiol.* **2014**, *12*, 35-48. DOI: 10.1038/nrmicro3155

8. Doudna, J. A.; Rath, V. L. Structure and Function of the Eukaryotic Ribosome: The Next Frontier. *Cell* **2002**, *109*, 153-156. DOI: 10.1016/S0092-8674(02)00725-0

9. Polacek, N.; Mankin A. S. The Ribosomal Peptidyl Transferase Center: Structure, Function, Evolution, Inhibition. *Crit Rev Biochem Mol Biol.* **2005**, *40*, 285-311. DOI: 10.1080/10409230500326334

10. Sohmen, D.; Harms, J. M.; Schlunzen, F.; Wilson, D. N. SnapShot: Antibiotic Inhibition of Protein Synthesis I. *Cell* **2009**, *138*, 1248-1248.e1.

11. Poehlsgaard, J.; Douthwaite, S. The Bacterial Ribosome as a Target for Antibiotics. *Nature Rev. Microbiol.* **2005**, *3*, 870-881. DOI: 10.1038/nrmicro1265

12. Xaplanteri, M. A.; Andreou, A.; Dinos, G. P.; Kalpaxis, D. L. Effect of Polyamines on the Inhibition of Peptidyltransferase by Antibiotics: Revisiting the Mechanism of Chloramphenicol Action. *Nucleic Acids Res.* **2003**, *31*, 5074-5083. DOI: 10.1093/nar/gkg686

13. Polacek, N; Gomez, M. J.; Ito, K.; Xiong, L.; Nakamura, Y.; Mankin, A. S. The Critical Role of the Universally Conserved A2602 of 23S Ribosomal RNA in the Release of the Nascent Peptide during Translation Termination. *Mol. Cell* **2003**, *11*, 103-112.

14. Thompson, J.; O'Connor, M.; Mills, J. A.; Dahlberg, A. E. The Protein Synthesis Inhibitors, Oxazolidinones and Chloramphenicol, Cause Extensive Translational Inaccuracy *in Vivo*. *J. Mol. Biol.* **2002**, *322*, 273-279. DOI: 10.1016/S0022-2836(02)00784-2

15. Myasnikov, A. G.; Natchiar, S. K.; Nebout, M.; Hazemann, I.; Imbert, V.; Khatter, H.; Peyron, J. F.; Klaholz, B. P. Structure-Function Insights Reveal the Human Ribosome as a Cancer Target for Antibiotics. *Nat. Commun.* **2016**, *7*, 12856. DOI: 10.1038/ncomms12856

16. Kalghatgi, S.; Spina, C. S.; Costello, J. C.; Liesa, M.; Morones-Ramirez, J. R.; Slomovic, S.; Molina, A.; Shirihai, O. S.; Collins, J. J. Bactericidal Antibiotics Induce Mitochondrial Dysfunction and Oxidative Damage in Mammalian Cells. *Sci. Transl. Med.*, 2013, 5, 192ra85. DOI: 10.1126/scitranslmed.3006055

17. Lamb, R.; Harrison, H.; Hulit, J.; Smith, D. L.; Lisanti, M. P.; Sotgia, F. Mitochondria as New Therapeutic Targets for Eradicating Cancer Stem Cells: Quantitative Proteomics and Functional Validation Via MCT1/2 Inhibition. *Oncotarget* **2014**, *5*, 11029-11037. DOI: 10.18632/oncotarget.2789

18. Killock, D. Drug Therapy: Can the Mitochondrial Adverse Effects of Antibiotics Be Exploited to Target Cancer Metabolism?. *Nature Rev. Clin. Onc.* **2015**, *12*, 190-190. DOI: 10.1038/nrclinonc.2015.24

19. Brown, D. Antibiotic Resistance Breakers: Can Repurposed Drugs Fill the Antibiotic Discovery Void?. *Nat. Rev. Drug Discov.* **2015**, *14*, 821-832. DOI: 10.1038/nrd4675

20. Esner, M.; Graifer, D.; Lleonart, M. E.; Lyakhovich, A. Targeting Cancer Cells Through Antibiotics-Induced Mitochondrial Dysfunction Requires Autophagy Inhibition. *Cancer Lett.* **2017**, *384*, 60-69. DOI: 10.1016/j.canlet.2016.09.023

21. Nguyen, L. V.; Vanner, R.; Dirks, P.; Eaves, C. J. Cancer Stem Cells: An Evolving Concept. *Nat. Rev. Cancer* **2012**, *12*, 133-143. DOI: 10.1038/nrc3184

22. Almora-Barrios, N.; De Leeuw, N. H. Molecular Dynamics Simulation of the Early Stages of Nucleation of Hydroxyapatite at a Collagen Template. *Cryst. Growth. Des.* **2012**, *12*, 756-763. DOI: 10.1021/cg201092s

23. Bertran, O.; del Valle, L. J.; Revilla-López, G.; Chaves, G.; Cardús, Ll.; Casas, M. T.; Casanovas, J.; Turon, P.; Puiggalí, J.; Alemán, C. Mineralization of DNA into

Nanoparticles of Hydroxyapatite. *Dalton Trans.* **2014**, *43*, 317-327. DOI: 10.1039/C3DT52112E

24. del Valle, L. J.; Bertran, O.; Chaves, G.; Revilla-López, G.; Rivas, M.; Casas, M. T.; Casanovas, J.; Turon, P.; Puiggalí, J.; Alemán, C. DNA Adsorbed on Hydroxyapatite Surfaces. *J. Mater. Chem. B* **2014**, *2*, 6953-6966. DOI: 10.1039/C4TB01184H

25. Kirkham, J.; Brookes, S. J.; Shore, R. C.; Wood, S. R.; Smith, D. A.; Zhang, J.; Chen, H.; Robinson, C. Physico-Chemical Properties of Crystal Surfaces in Matrix–Mineral Interactions During Mammalian Biomineralisation. *Curr. Opin. Colloid Interface Sci.* **2002**, *7*, 124-132. DOI: 10.1016/S1359-0294(02)00017-1

26. Almora-Barrios, N.; Austen, K. F.; de Leeuw, N. H. Density Functional Theory Study of the Binding of Glycine, Proline, and Hydroxyproline to the Hydroxyapatite (0001) and ($01\bar{1}0$) Surfaces. *Langmuir* **2009**, *25*, 5018-5025. DOI: 10.1021/la803842g

27. Rivas, M.; Casanovas, J.; del Valle, L. J.; Bertran, O.; Revilla-López, G.; Turon, P.; Puiggalí, J.; Alemán, C. An Experimental-Computer Modeling Study of Inorganic Phosphates Surface Adsorption on Hydroxyapatite Particles. *Dalton Trans.* **2015**, *44*, 9980-9991. DOI: 10.1039/C5DT00209E

28. Doi, K.; Kubi, T.; Takeshita, R.; Kajihara, S.; Kato, S.; Kawazoe, Y.; Shiba, T.; Akagawa, Y. Inorganic Polyphosphate Adsorbed onto Hydroxyapatite for Guided Bone Regeneration: An Animal Study. *Dent. Mater. J.* **2014**, *33*, 179-186. DOI: 10.4012/dmj.2013-275

29. Comeau, P. A.; Frei, H.; Yang, C.; Fernlund, G.; Rossi, F. M. In Vivo Evaluation of Calcium Polyphosphate for Bone Regeneration. *J. Biomater. Appl.* **2012**, *27*, 267-275. DOI: 10.1177/0885328211401933

30. Jeon, B. J.; Jeong, S. Y.; Koo, A. N.; Kim, B. C.; Hwang, Y. S.; Lee, S. C. Fabrication of Porous PLGA Microspheres with BMP-2 Releasing Polyphosphate-Functionalized Nano-Hydroxyapatite for Enhanced Bone Regeneration. *Macromol. Res.* **2012**, *20*, 715-724. DOI: 10.1007/s13233-012-0103-5

31. Morita, K.; Doi, K.; Kubo, T.; Takeshita, R.; Kato, S.; Akagawa, Y. Enhanced Initial Bone Regeneration with Inorganic Polyphosphate-Adsorbed Hydroxyapatite. *Acta Biomater.* **2010**, *6*, 2808-2815. DOI: 10.1016/j.actbio.2009.12.055

32. Kamat, S. S.; Raushel, F. M. The Enzymatic Conversion of Phosphonates to Phosphate by Bacteria. *Curr. Opin. Chem. Biol.* **2013**, *17*, 589-596. DOI: 10.1016/j.cbpa.2013.06.006

33. Russell, R. G. G.; Ebetino, F. H. Mechanisms of Action of Bisphosphonates: Similarities and Differences and their Potential Influence on Clinical Efficacy. *Osteoporos. Int.* **2008**, *19*, 733-759. DOI: 10.1007/s00198-007-0540-8

34. Uskokovic, V.; Uskokovic, D. P. Nanosized Hydroxyapatite and Other Calcium Phosphates: Chemistry of Formation and Application as Drug and Gene Delivery Agents. *J. Biomed. Mater. Res., Part B* **2011**, *96*, 152-191. DOI: 10.1002/jbm.b.31746.

35. Olton, D.; Li, J.; Wilson, M. E.; Rogers, T.; Close, J.; Huang, L.; Kumta, N. P.; Sfeir, C. Nanostructured Calcium Phosphates (NanoCaPs) for Non-Viral Gene Delivery: Influence of the Synthesis Parameters on Transfection Efficiency. *Biomaterials* **2007**, *28*, 1267-1279. DOI: 10.1016/j.biomaterials.2006.10.026

36. Waldon, J.; Kubicek, M. R.; Johnson, G. A.; Buhl, A. E. A HPLC-Based Chloramphenicol Acetyltransferase Assay for Assessing Hair Growth: Comparison of the Sensitivity of UV and Fluorescence Detection. *Eur. J. Clin. Chem. Clin. Biochem.* **1993**, *31*, 41-45. DOI: 10.1515/cclm.1993.31.1.41

37. Suzuky, M.; Shindo M. Studies on the Infrared Spectra of Stereoisomers. The Infrared Spectra of Chloramphenicol and Related Compounds. *J. Pharm. Soc. Jpn.* **1956**, **76**, 927-931. DOI: 10.1248/yakushi1947.76.8_927

38. Dunitz, J. D. The Crystal Structure of Chloramphenicol[1] and Bromamphenicol[2]. *J. Am. Chem. Soc.* **1952**, *74*, 995-999. DOI: 10.1021/ja01124a037

39. Ravindra Acharya, K.; Sake Gowda, D. S.; Post, M. The Structure of Chloramphenicol. *Acta Cryst.* **1979**, *B35*, 1360-1363. DOI: 10.1107/S0567740879006312

40. Bulkley, D.; Innis, C. A.; Blaha, G.; Steitz, T. A. Revisiting the Structures of Several Antibiotics Bound to the Bacterial Ribosome. *Proc. Natl. Acad. Sci.* **2010**, *107*, 17158-17163. DOI: 10.1073/pnas.1008685107

41. Wright, D. Bacterial Resistance to Antibiotics: Enzymatic Degradation and Modification. *Adv. Drug Deliv. Rev.* **2005**, *57*, 1451-1470. DOI: 10.1016/j.addr.2005.04.002

42. Motskin, M.; Wright, D. M.; Muller, K.; Kyle, N.; Gard, T. G.; Porter, A. E.; Skepper, J. N. Hydroxyapatite Nano and Microparticles: Correlation of Particle Properties with Cytotoxicity and Biostability. *Biomaterials* **2009**, *30*, no. 3307-3317. DOI: 10.1016/j.biomaterials.2009.02.044

43. Zhang, H.; Qing, F.; Zhao, F.; Hongsong, F.; Liu, M.; Zhang, X. Cellular Internalization of Rod-Like Nano Hydroxyapatite Particles and Their Size and Dose-Dependent Effects on Pre-osteoblasts. *J. Mat. Chem. B* **2017**, *5*, 1205-1217. DOI: 10.1039/C6TB01401A

44. Bauer, I. W.; Li, S.; Han, Y.; Yuan, L.; Yin, M. Internalization of Hydroxyapatite Nanoparticles in Liver Cancer Cells. *J. Mater. Sci. Mater. Sci.* **2008**, *19*, 1091-1095. DOI: 10.1007/s10856-007-3124-4

45. Sutherland, R.; Delia, D.; Schneider, C.; Newman, R.; Kemshead, J.; Greaves M. Ubiquitous Cell-Surface Glycoprotein on Tumor Cells Is Proliferation-Associated Receptor for Transferrin. *Proc. Natl. Acad. Sci. U.S.A.* **1981**, *78*, 4515-4519.

46. Daniels, T. R.; Delgado, T.; Rodriguez, J. A.; Helguera, G.; Penichet, M. L. The Transferrin Receptor Part I: Biology and Targeting with Cytotoxic Antibodies for the Treatment of Cancer. *Clin. Immunol*. **2006**, *121*, 144-158. DOI: 10.1016/j.clim.2006.06.010

47. Daniels, T. R.; Delgado, T.; Helguera, G.; Penichet, M. L. The Transferrin Receptor Part II: Targeted Delivery of Therapeutic Agents Into Cancer. *Clin. Immunol*. **2006**, *121*, 159-176. DOI: 10.1016/j.clim.2006.06.006

Table 1. Crystallinity (χ_c) and crystallite size (L) of the unloaded and CHL-loaded mineral samples.

	χ_c	L (nm)
cHAp	0.66±0.03	57±2
CAM(Ca)/HAp	0.20±0.02	36±2
ACP	0.10±0.02	7±1
CAM(Ca)/ACP	0.06±0.01	6±1

CAPTIONS TO FIGURES

Figure 1. (a) Scheme to illustrate the four *in situ* synthetic strategies used to prepare CAM-loaded mineral NPs: CAM(Pho)/cHAp, CAM(Pho)/ACP, CAM(Ca)/cHAP and CAM(Ca)/ACP. (b) Distribution of the antibiotic loaded *in situ* during the synthesis of cHAp and ACP NPs using the Pho- and Ca-paths. The amount of antibiotic adsorbed onto the surface and encapsulated into the matrix has been evaluated separately (see text). The total amount of loaded CAM corresponds to the sum of adsorbed and encapsulated. The loading ratio is expressed with respect to the weight of dry mineral.

Figure 2. (a) Selected regions of the FTIR spectra of **C**AM, cHAp, CAM(Ca)/cHAp as prepared (with both adsorbed and encapsulated CAM), and CAM(Ca)/cHAp after washing with PBS-EtOH (with encapsulated CAM only). (b) X-ray diffraction patterns of unloaded and CAM(Ca)-loaded cHAp and ACP samples as prepared.

Figure 3. SEM (left) and TEM (right) images of (a) CAM crystals, (b) CAM(Ca)/ACP and (c) CAM(Ca)/cHAp NPs after washing with PBS-EtOH (loaded with encapsulated CA only).

Figure 4. SEM images of CAM(Ca)-loaded ACP (left) and cHAp (right) NPs after incubation with (a) polyP, (b) $P_2O_7^{4-}$ and (c) ATMP aqueous solutions. The arrows indicate the presence of crystals of the bioadsorbed compounds.

Figure 5. Inhibition of *E. coli* growth by CAM. Results are expressed as a percentage of the control against the logarithm concentration of antibiotic for: (a) free CAM, CAM(Ca)/cHAp and CAM(Ca)/ACP; (b) uncoated and biocoated CAM(Ca)/cHAp NPs; and (c) uncoated and biocoated CAM(Ca)/ACP NPs.

Figure 6. Antibiotic release profiles in PBS for (a) uncoated, (b) polyP coated, (c) $P_2O_7^{4-}$ coated and (d) ATMP coated CAM(Ca)-loaded cHAp and ACP NPs. CAM-

incubated samples (uncoated and biocoated CAM(c)/cHAp and CAM(c)/ACP NPs) were used as control NPs.

Figure 7. Antibiotic release profiles in different cell culture media (HUVEC, COS-1 and MCF-7 cell lines) for (a) uncoated CAM(Ca)/cHAp, (b) uncoated CAM(Ca)/ACP, (c) CAM(Ca)/cHAp coated with polyP, and (d) CAM(Ca)/ACP coated with polyP. CAM-incubated samples, CAM(c)/cHAp and CAM(c)/ACP, were used as control. Results obtained for NPs coated with $P_2O_7^{4-}$ and ATMP are displayed in Figure S11.

Figure 8. Cytotoxicity curves of CAM. Cell viability of HUVEC, COS-1 and MCF-7 cells with increasing concentration of CAM (in μM) evaluated at (a) 24 h and (b) 48 h of culture. Curves are expressed as percentage of surviving cells relative to the control against the logarithm of CAM concentration.

Figure 9. Temporal variation of the percentage of surviving cells after the incorporation of uncoated and biocoated CAM(Ca)/cHAp NPs to electroporated (a) HUVEC, (b) COS-1 and (c) MCF-7 cells, and (d) CAM(c)/cHAp NPs to electroporated MCF-7 cells.

Figure 10. Temporal variation of the percentage of surviving cells after the incorporation of uncoated and biocoated CAM(Ca)/cHAp NPs to non-electroporated (a) HUVEC, (b) COS-1, (c) MCF-7 and (d) MIA PaCa-2 cells.

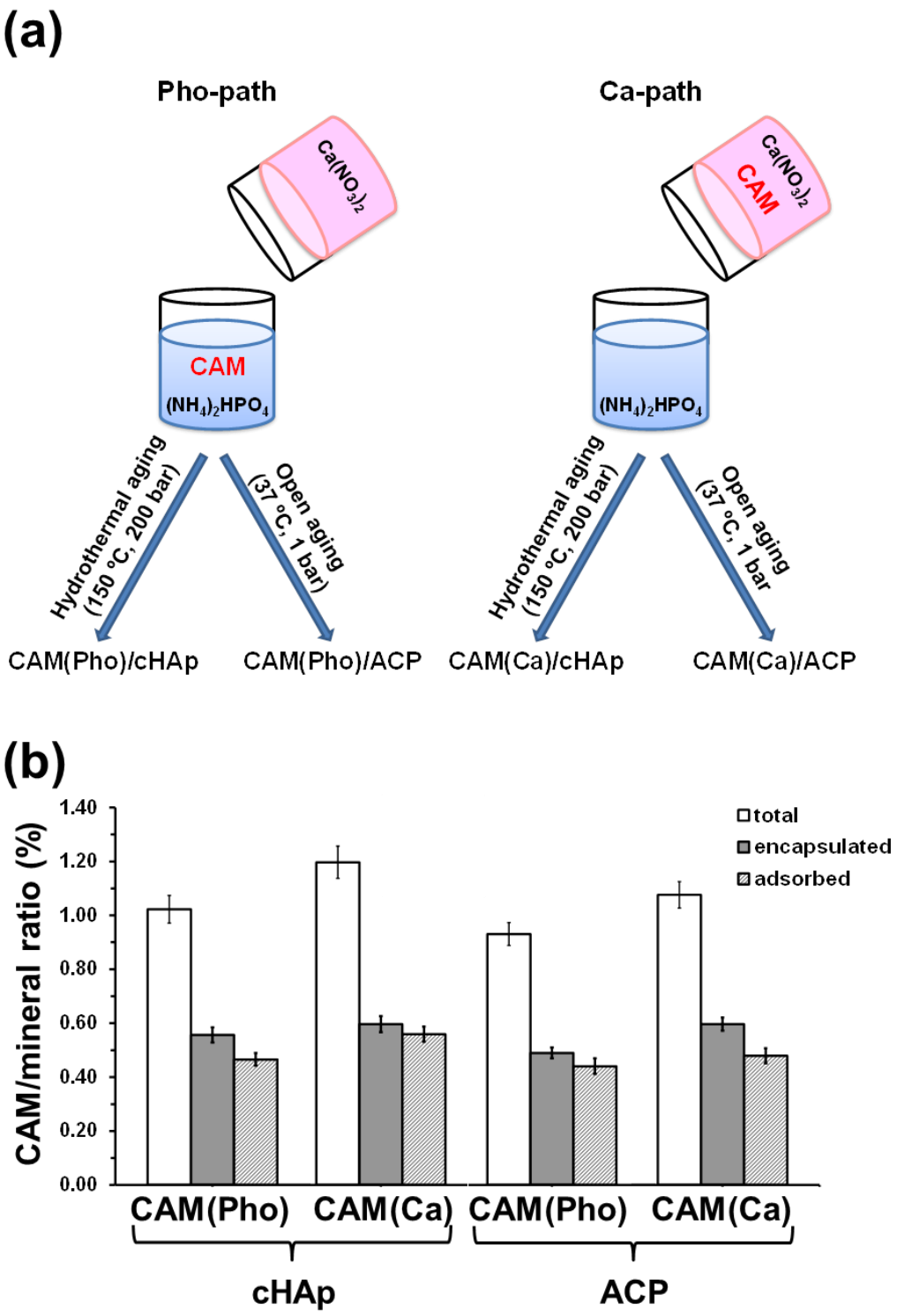
(a)
Pho-path
Ca-path
Ca(NO3)2
CAM
(NH4)2HPO4
Hydrothermal aging
(150 °C, 200 bar)
Open aging
(37 °C, 1 bar)
CAM(Pho)/cHAp
CAM(Pho)/ACP
CAM(Ca)/cHAp
CAM(Ca)/ACP
(b)
CAM/mineral ratio (%)
1.40
1.20
1.00
0.80
0.60
0.40
0.20
0.00
total
encapsulated
adsorbed
CAM(Pho)
CAM(Ca)
CAM(Pho)
CAM(Ca)
cHAp
ACP

Figure 1

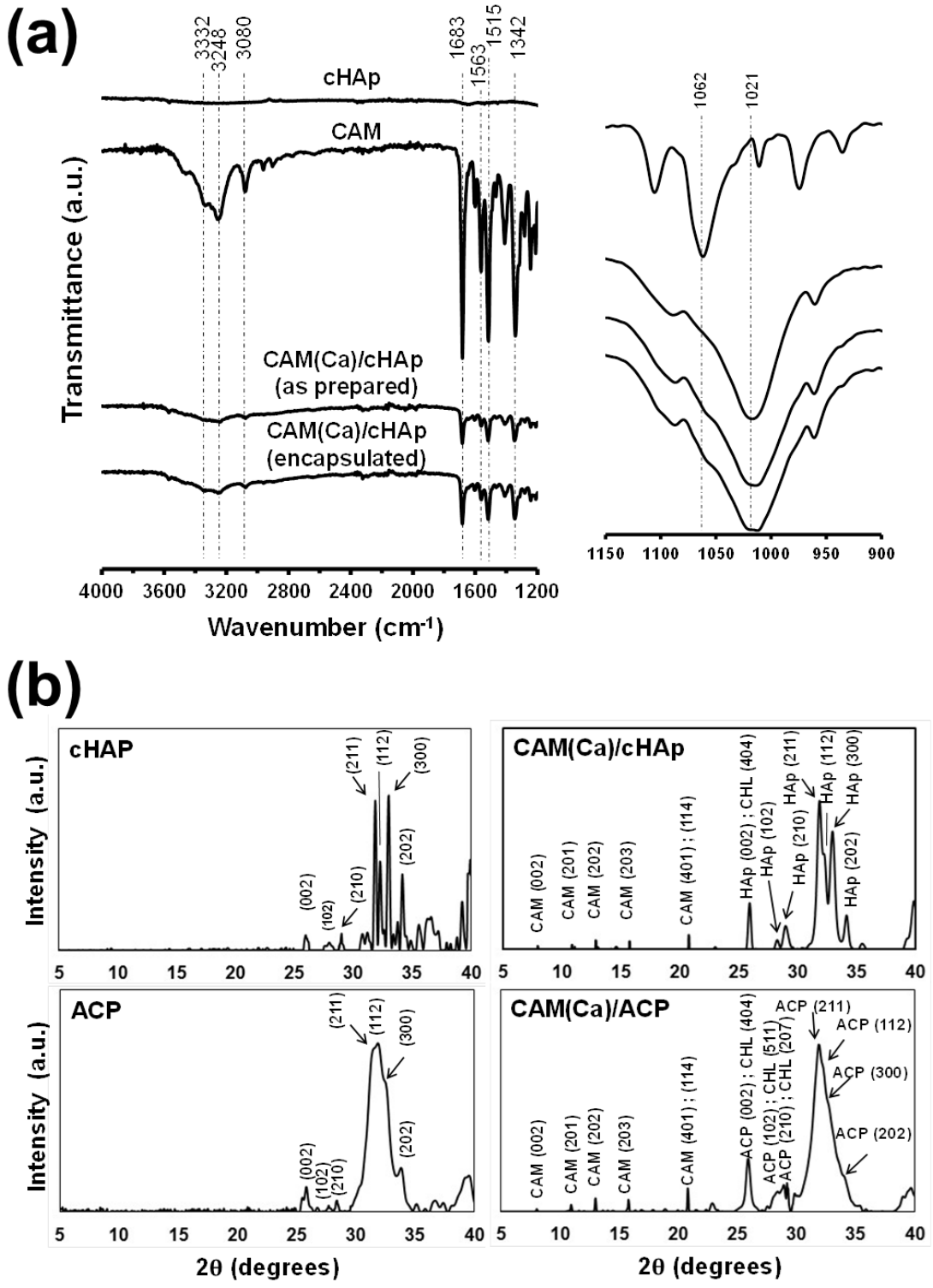
(a)
3332
3248
3080
1683
1563
1515
1342
cHAp
CAM
CAM(Ca)/cHAp
(as prepared)
CAM(Ca)/cHAp
(encapsulated)
Transmittance (a.u.)
4000 3600 3200 2800 2400 2000 1600 1200
Wavenumber (cm-1)
1062
1021
1150 1100 1050 1000 950 900
(b)
cHAP
(002)
(102)
(210)
(211)
(112)
(300)
(202)
CAM(Ca)/cHAp
CAM (002)
CAM (201)
CAM (202)
CAM (203)
CAM (401) ; (114)
HAp (002) ; CHL (404)
HAp (102)
HAp (210)
HAp (211)
HAp (112)
HAp (300)
HAp (202)
ACP
CAM(Ca)/ACP
ACP (002) ; CHL (404)
ACP (102) ; CHL (511)
ACP (210) ; CHL (207)
ACP (211)
ACP (112)
ACP (300)
ACP (202)
Intensity (a.u.)
5 10 15 20 25 30 35 40
2θ (degrees)

Figure 2

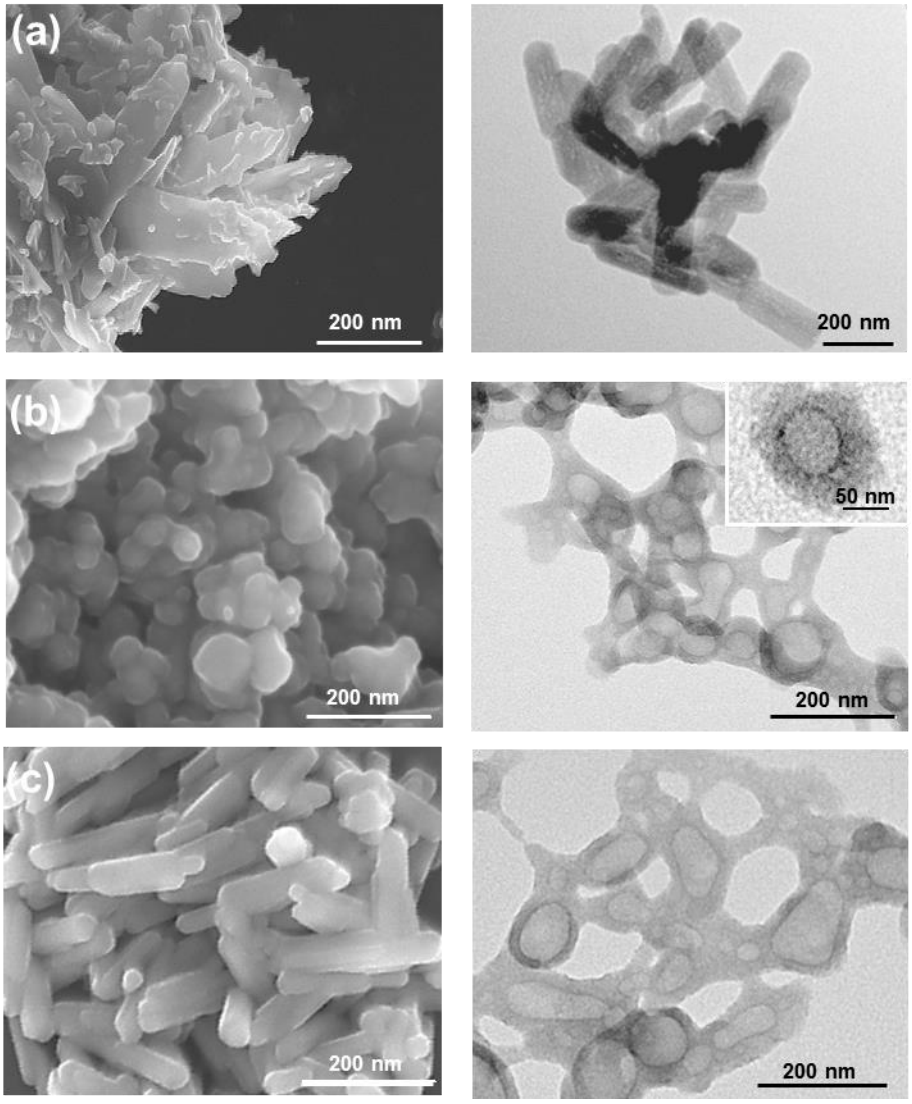

Figure 3

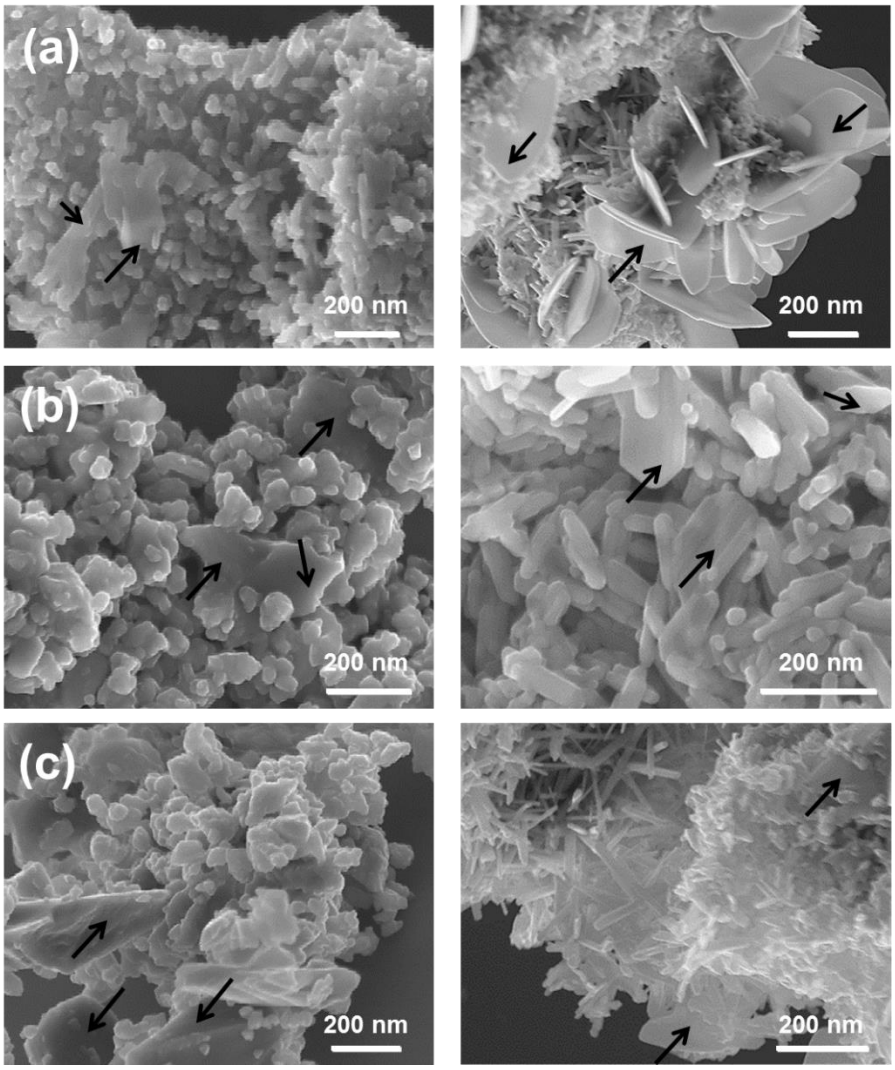

Figure 4

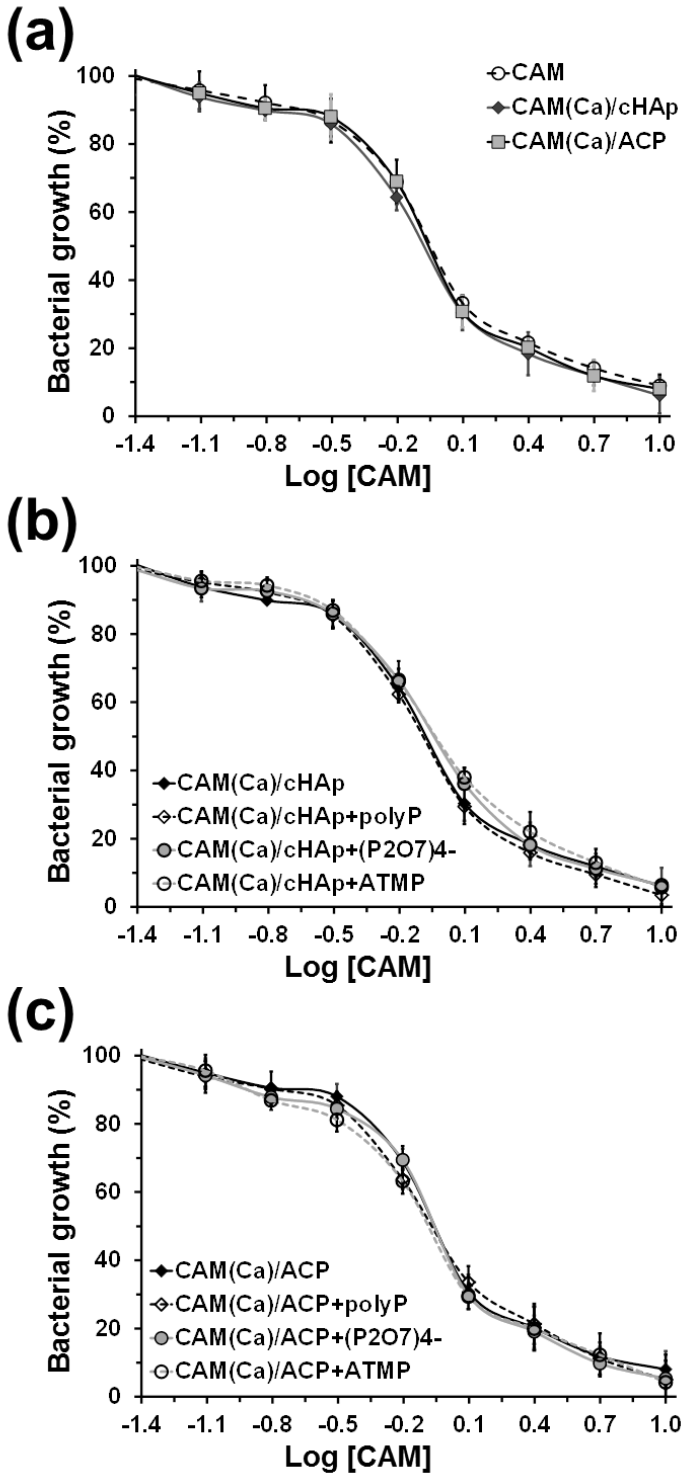
(a)
CAM
CAM(Ca)/cHAp
CAM(Ca)/ACP
Bacterial growth (%)
Log [CAM]
(b)
CAM(Ca)/cHAp
CAM(Ca)/cHAp+polyP
CAM(Ca)/cHAp+(P2O7)4-
CAM(Ca)/cHAp+ATMP
Bacterial growth (%)
Log [CAM]
(c)
CAM(Ca)/ACP
CAM(Ca)/ACP+polyP
CAM(Ca)/ACP+(P2O7)4-
CAM(Ca)/ACP+ATMP
Bacterial growth (%)
Log [CAM]

Figure 5

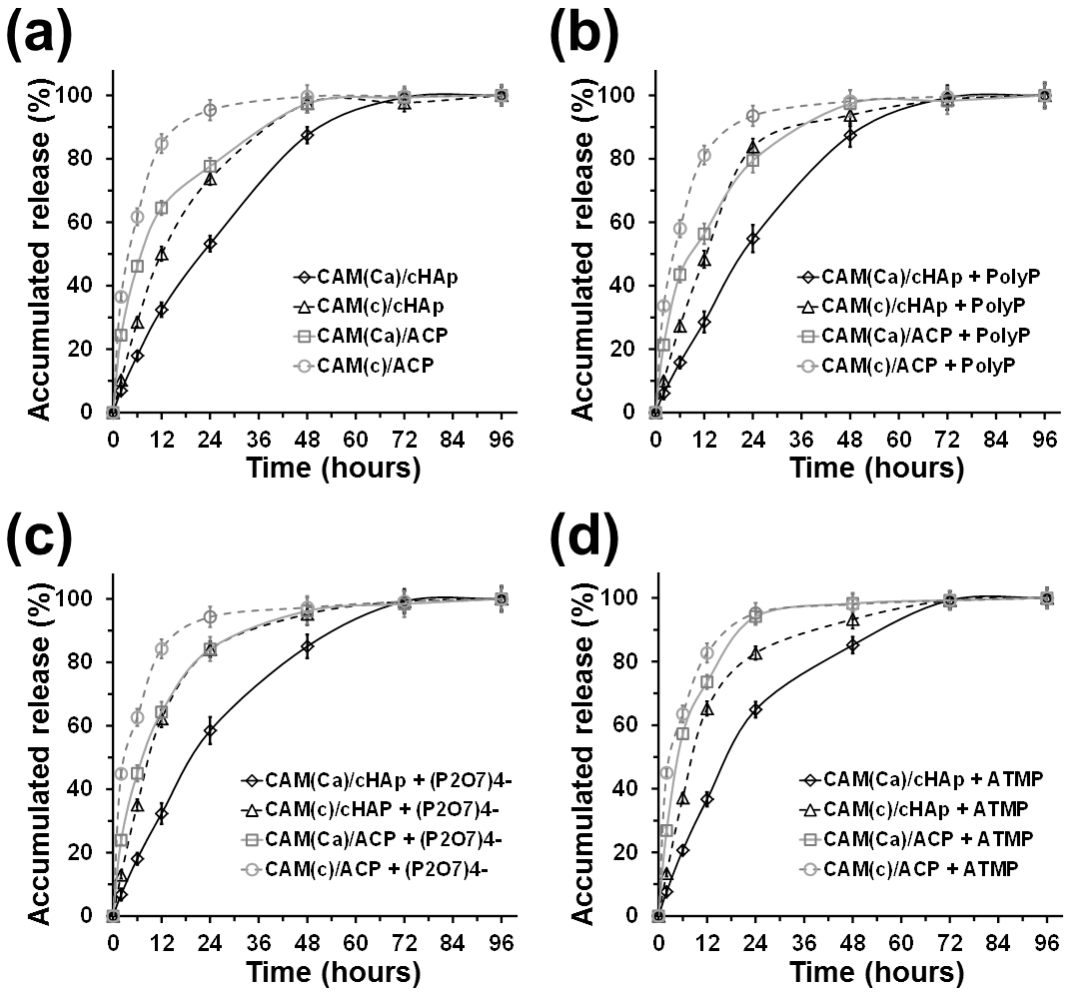
(a)
Accumulated release (%)
Time (hours)
CAM(Ca)/cHAp
CAM(c)/cHAp
CAM(Ca)/ACP
CAM(c)/ACP
(b)
Accumulated release (%)
Time (hours)
CAM(Ca)/cHAp + PolyP
CAM(c)/cHAp + PolyP
CAM(Ca)/ACP + PolyP
CAM(c)/ACP + PolyP
(c)
Accumulated release (%)
Time (hours)
CAM(Ca)/cHAp + (P2O7)4-
CAM(c)/cHAP + (P2O7)4-
CAM(Ca)/ACP + (P2O7)4-
CAM(c)/ACP + (P2O7)4-
(d)
Accumulated release (%)
Time (hours)
CAM(Ca)/cHAp + ATMP
CAM(c)/cHAp + ATMP
CAM(Ca)/ACP + ATMP
CAM(c)/ACP + ATMP

Figure 6

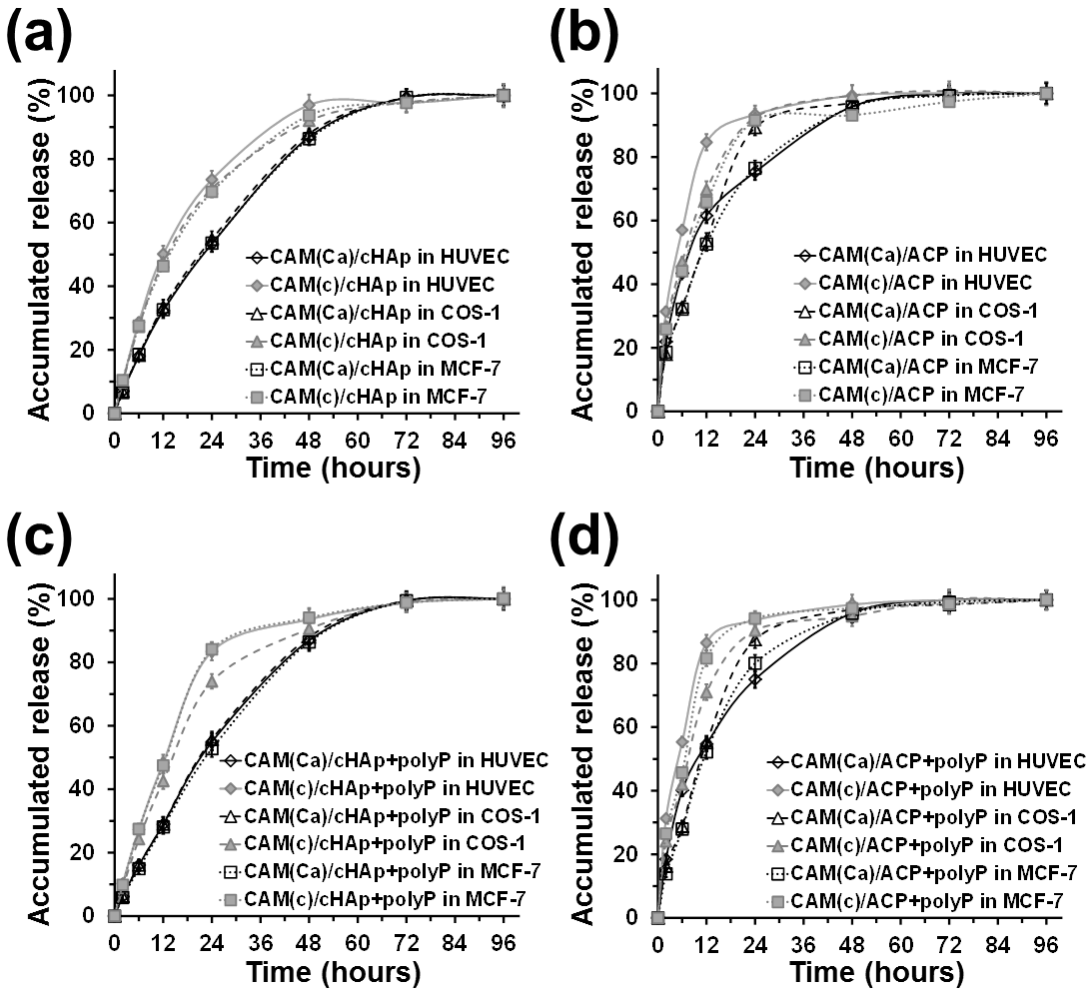
(a)
Accumulated release (%)
Time (hours)
CAM(Ca)/cHAp in HUVEC
CAM(c)/cHAp in HUVEC
CAM(Ca)/cHAp in COS-1
CAM(c)/cHAp in COS-1
CAM(Ca)/cHAp in MCF-7
CAM(c)/cHAp in MCF-7
(b)
Accumulated release (%)
Time (hours)
CAM(Ca)/ACP in HUVEC
CAM(c)/ACP in HUVEC
CAM(Ca)/ACP in COS-1
CAM(c)/ACP in COS-1
CAM(Ca)/ACP in MCF-7
CAM(c)/ACP in MCF-7
(c)
Accumulated release (%)
Time (hours)
CAM(Ca)/cHAp+polyP in HUVEC
CAM(c)/cHAp+polyP in HUVEC
CAM(Ca)/cHAp+polyP in COS-1
CAM(c)/cHAp+polyP in COS-1
CAM(Ca)/cHAp+polyP in MCF-7
CAM(c)/cHAp+polyP in MCF-7
(d)
Accumulated release (%)
Time (hours)
CAM(Ca)/ACP+polyP in HUVEC
CAM(c)/ACP+polyP in HUVEC
CAM(Ca)/ACP+polyP in COS-1
CAM(c)/ACP+polyP in COS-1
CAM(Ca)/ACP+polyP in MCF-7
CAM(c)/ACP+polyP in MCF-7

Figure 7

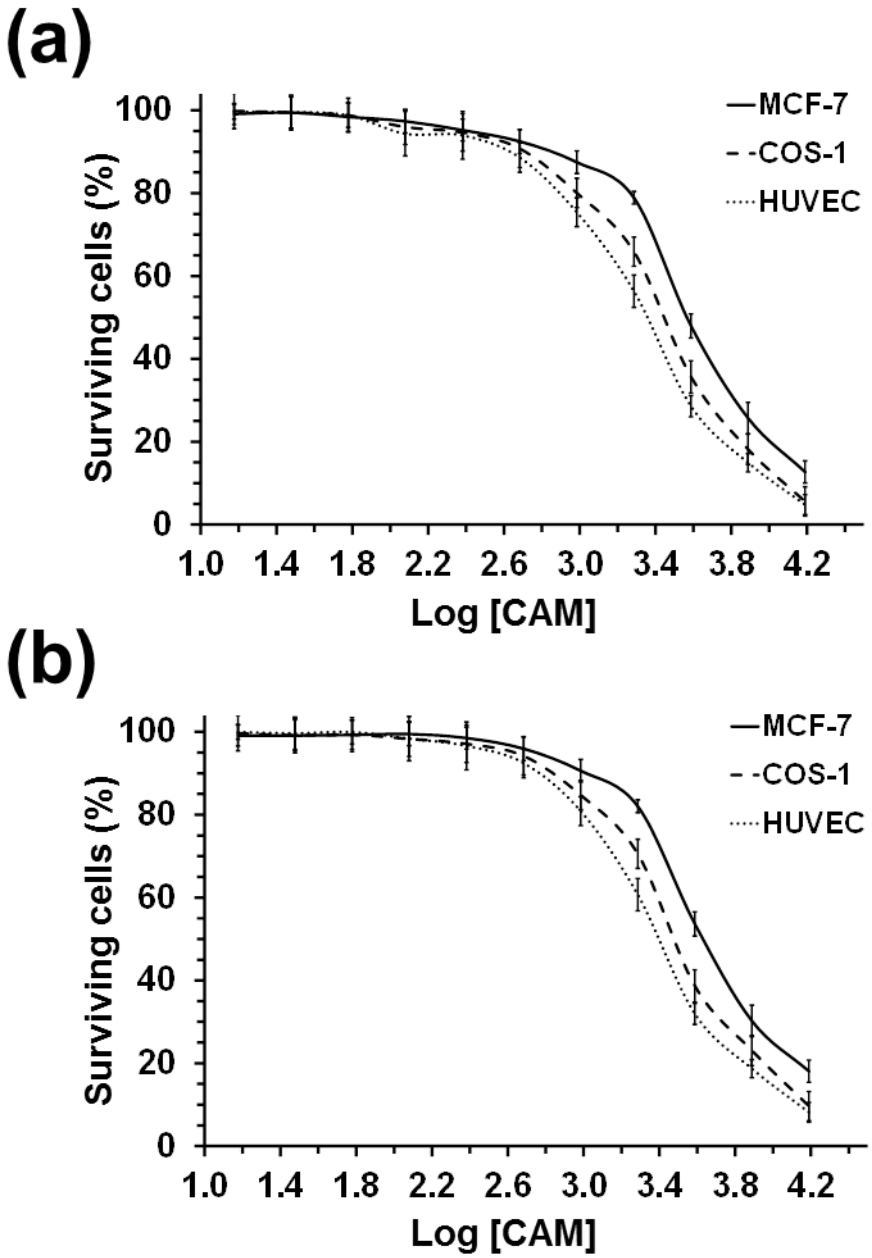
(a)
100
80
60
40
20
0
Surviving cells (%)
1.0 1.4 1.8 2.2 2.6 3.0 3.4 3.8 4.2
Log [CAM]
MCF-7
COS-1
HUVEC
(b)
100
80
60
40
20
0
Surviving cells (%)
1.0 1.4 1.8 2.2 2.6 3.0 3.4 3.8 4.2
Log [CAM]
MCF-7
COS-1
HUVEC

Figure 8

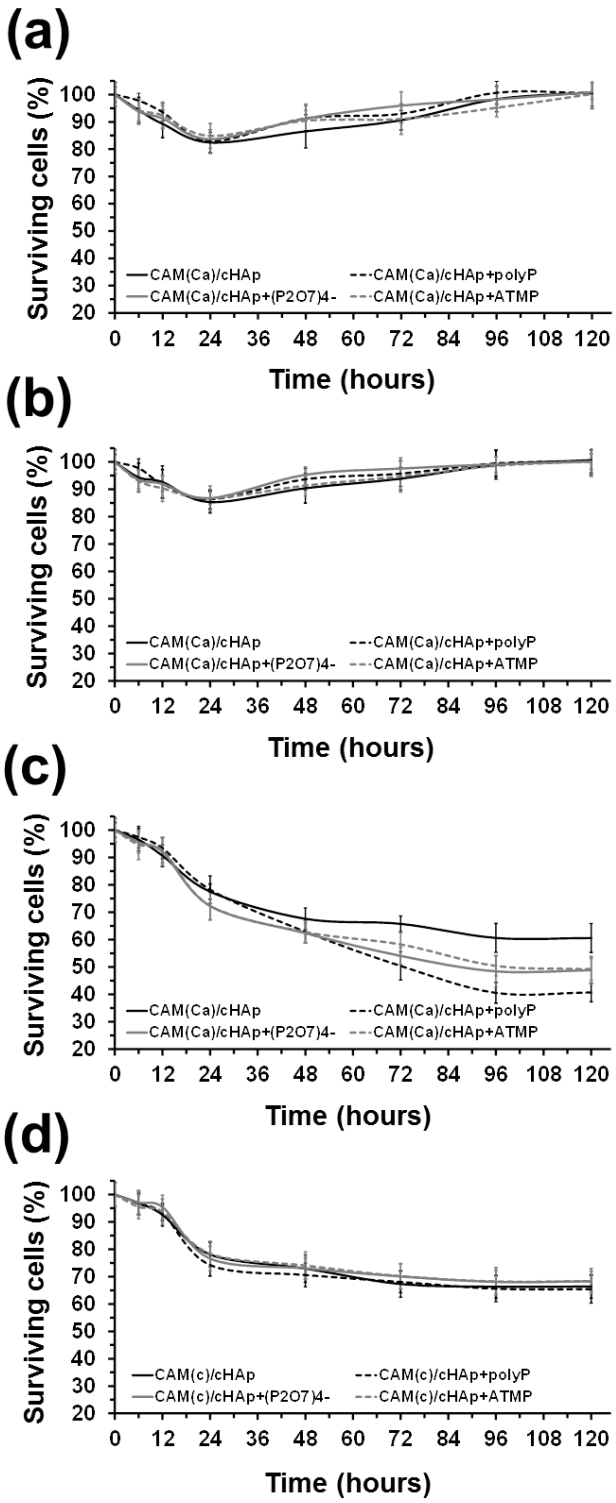
(a)
Surviving cells (%)
100
90
80
70
60
50
40
30
20
0 12 24 36 48 60 72 84 96 108 120
Time (hours)
CAM(Ca)/cHAp
CAM(Ca)/cHAp+polyP
CAM(Ca)/cHAp+(P2O7)4-
CAM(Ca)/cHAp+ATMP
(b)
Surviving cells (%)
100
90
80
70
60
50
40
30
20
0 12 24 36 48 60 72 84 96 108 120
Time (hours)
CAM(Ca)/cHAp
CAM(Ca)/cHAp+polyP
CAM(Ca)/cHAp+(P2O7)4-
CAM(Ca)/cHAp+ATMP
(c)
Surviving cells (%)
100
90
80
70
60
50
40
30
20
0 12 24 36 48 60 72 84 96 108 120
Time (hours)
CAM(Ca)/cHAp
CAM(Ca)/cHAp+polyP
CAM(Ca)/cHAp+(P2O7)4-
CAM(Ca)/cHAp+ATMP
(d)
Surviving cells (%)
100
90
80
70
60
50
40
30
20
0 12 24 36 48 60 72 84 96 108 120
Time (hours)
CAM(c)/cHAp
CAM(c)/cHAp+polyP
CAM(c)/cHAp+(P2O7)4-
CAM(c)/cHAp+ATMP

Figure 9

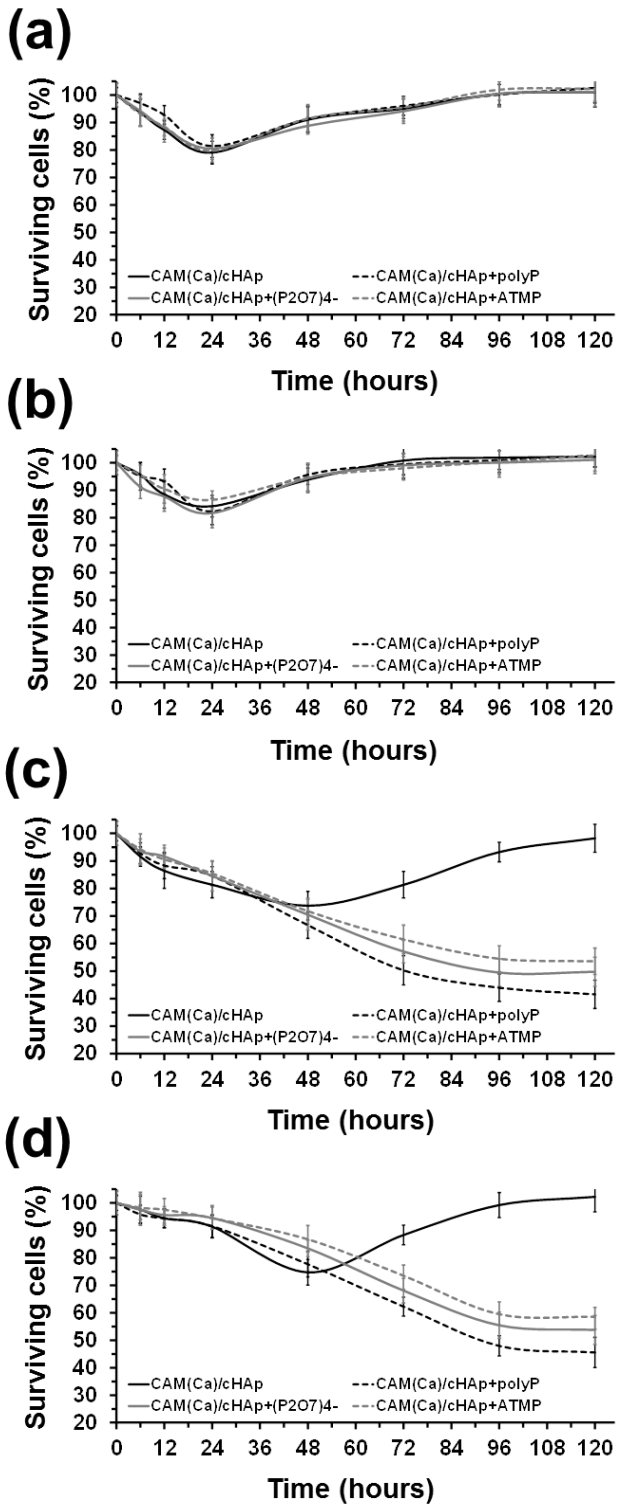
(a)
Surviving cells (%)
100
90
80
70
60
50
40
30
20
0 12 24 36 48 60 72 84 96 108 120
Time (hours)
CAM(Ca)/cHAp
CAM(Ca)/cHAp+polyP
CAM(Ca)/cHAp+(P2O7)4-
CAM(Ca)/cHAp+ATMP
(b)
Surviving cells (%)
100
90
80
70
60
50
40
30
20
0 12 24 36 48 60 72 84 96 108 120
Time (hours)
CAM(Ca)/cHAp
CAM(Ca)/cHAp+polyP
CAM(Ca)/cHAp+(P2O7)4-
CAM(Ca)/cHAp+ATMP
(c)
Surviving cells (%)
100
90
80
70
60
50
40
30
20
0 12 24 36 48 60 72 84 96 108 120
Time (hours)
CAM(Ca)/cHAp
CAM(Ca)/cHAp+polyP
CAM(Ca)/cHAp+(P2O7)4-
CAM(Ca)/cHAp+ATMP
(d)
Surviving cells (%)
100
90
80
70
60
50
40
30
20
0 12 24 36 48 60 72 84 96 108 120
Time (hours)
CAM(Ca)/cHAp
CAM(Ca)/cHAp+polyP
CAM(Ca)/cHAp+(P2O7)4-
CAM(Ca)/cHAp+ATMP

Figure 10

GRAPHICAL ABSTRACT